Metabolic Atlas of Human Eyelid Infiltrative Basal Cell Carcinoma

Yanjing Huang, Chengjie He, Qiuling Hu, Zhong Liu, Xingyi Li, Wuyou Gao, Xuanwei Liang, Rongxin Chen, Zhen Mao, and Xianchai Lin

State Key Laboratory of Ophthalmology, Zhongshan Ophthalmic Center, Sun Yat-Sen University, Guangdong Provincial Key Laboratory of Ophthalmology and Visual Science, Guangzhou, China

Correspondence: Rongxin Chen, State Key Laboratory of Ophthalmology, Zhongshan Ophthalmic Center, Sun Yat-Sen University, Guangdong Provincial Key Laboratory of Ophthalmology and Visual Science, Guangzhou 510060, China; chenrx25@mail.sysu.edu.cn.
Zhen Mao, State Key Laboratory of Ophthalmology, Zhongshan Ophthalmic Center, Sun Yat-Sen University, Guangdong Provincial Key Laboratory of Ophthalmology and Visual Science, Guangzhou 510060, China; ophmaozhen@gmail.com.
Xianchai Lin, State Key Laboratory of Ophthalmology, Zhongshan Ophthalmic Center, Sun Yat-Sen University, Guangdong Provincial Key Laboratory of Ophthalmology and Visual Science, Guangzhou 510060, China; linxch7@mail.sysu.edu.cn.

YH and CH contributed equally to this article.

Received: August 4, 2024
Accepted: December 5, 2024
Published: January 7, 2025

Citation: Huang Y, He C, Hu Q, et al. Metabolic atlas of human eyelid infiltrative basal cell carcinoma. *Invest Ophthalmol Vis Sci.* 2025;66(1):11. https://doi.org/10.1167/iovs.66.1.11

Purpose. Eyelid infiltrative basal cell carcinoma (iBCC) is the most common malignant tumor affecting the ocular adnexa, but studies on metabolic changes within its microenvironment and heterogeneity at the tumor invasive area are limited. This study aims to analyze metabolic differences among iBCC cell types using single-cell and spatial metabolomics analysis and to examine metabolic environment at the tumor invasive area.

Methods. Single-cell transcriptomic data of human basal cell carcinoma (BCC) were clustered and visualized using Uniform Manifold Approximation and Projection. Metabolic reprogramming was analyzed with single-cell flux estimation analysis. Spatial metabolomics data were obtained with the Timstof Flex MALDI 2 system, and Bruker software was used for region selection.

Results. Eight cell types were identified within the iBCC microenvironment. Differences between inflammatory cancer-associated fibroblasts and myofibroblastic cancer-associated fibroblasts were analyzed. Metabolic flux analysis showed increased glycolysis, glutamine, heme, and glutathione fluxes in the iBCC microenvironment. Spatial metabolomics revealed high levels of taurine, deoxy-GMP, O-phosphoethanolamine, and pyrithione. Both tumor and invasive regions had significant upregulation of fatty acid pathways, with marked increases in oleic and arachidonic acids at the invasive area. Specific upregulation of UDP-glucuronic acid and high UDP-glucose 6-dehydrogenase (UGDH) expression in the tumor region suggest UXS1 as a potential therapeutic target for iBCC.

Conclusions. This study establishes a metabolic microenvironment atlas of iBCC, revealing significant metabolic differences and the dominance of lipid and lysosome metabolism. Potential metabolic markers and characteristic substances in the invasive area offer new insights for immunotherapy and the exploration of BCC's metabolic mechanisms.

Keywords: eyelid infiltrative basal cell carcinoma, mass spectrometry imaging, tumor microenvironment, metabolic reprogramming, single-cell sequencing

Basal cell carcinoma (BCC) of the eyelid is the most common malignant tumor affecting ocular adnexa, accounting for approximately 85% to 95% of eyelid malignancies.[1] It primarily affects elderly individuals over 60 years old. Although BCC has a relatively low mortality rate, its lifetime risk reaches 20% to 30%.[2] The incidence rate of BCC is increasing globally, with a particularly significant rise observed in Asian regions.[3] Concurrently, there is a worldwide trend toward younger-onset ages.[4,5] This shift not only impacts public health but also imposes a substantial economic burden, as the associated medical costs are significant and cannot be underestimated.

Over 80% of BCCs occur in the head and neck region, with 20% occurring around the eyes. In the periocular area, common affected sites include the upper and lower eyelids, as well as the inner and outer canthus.[1] BCCs are a heterogeneous group of tumors that include superficial, nodular, ulcerated, and infiltrative types.[6,7] Infiltrative BCC (iBCC) is a particularly aggressive subtype that often leads to skin ulcers and invades surrounding tissues such as the orbit,[8] cornea,[9] and lacrimal apparatus.[10]

Common treatments for eyelid BCC include surgery and radiotherapy, with the standard approach being controlled lesion excision followed by eyelid reconstruction.[11] While

Copyright 2025 The Authors

This work is licensed under a Creative Commons Attribution-NonCommercial-NoDerivatives 4.0 International License.

surgical excision can be highly effective, it is less standardized than Mohs micrographic surgery,[12] and local recurrence rates can reach up to 20%.[13] This risk is even higher in infiltrative cases, which are more prone to postoperative recurrence. According to European consensus guidelines for BCC, approximately 10% of cases are considered "difficult to treat" due to factors such as large tumor size, challenging locations (e.g., near the eyes, nose, lips, or ears), poorly defined borders, recurrence, or patient-specific factors like comorbidities or reluctance to undergo surgery.[6] In such cases, patients with locally advanced eyelid BCC or metastatic BCC may require alternative therapies, including hedgehog pathway inhibitors (e.g., vismodegib or sonidegib)[14,15] and immune checkpoint inhibitors (e.g., PD-1).[15] However, these options are limited by high costs and issues with drug resistance.[16]

Research on BCC has advanced to the tumor microenvironment. Studies show that cancer-associated fibroblasts (CAFs) regulate the PTEN/PI3K/Akt pathway by overexpressing fibroblast activation protein, which downregulates PTEN, inhibits apoptosis, and promotes CAF proliferation, thus supporting tumor growth.[17] Also, CAFs activated WNT5A to maintain inflammation, while tumors release heat shock proteins to adapt and promote proliferation.[17] This phenomenon led us to recognize the substantial potential role of CAFs in iBCC. As a subtype related closely to tumor microenvironment,[18] we believed that exploring the interactions between CAFs and iBCC cells could yield valuable insights into the mechanisms driving tumor progression and treatment resistance.

Besides, previous liquid chromatography/tandem mass spectrometry (MS) studies identified 16 metabolites with changes in NAD, glutathione, polyamine, and amino acid metabolism in BCC samples.[19] Building on these findings, we speculate that metabolic changes in iBCC contribute significantly to its pathological alterations. Our primary goal is to identify metabolic biomarkers that can assist in the early diagnosis and treatment of iBCC. Additionally, we aim to trace the dynamic metabolic shifts in iBCC as it progresses from adjacent skin to the tumor invasion zone and ultimately to the tumor core. This comprehensive approach will help illuminate the mechanisms driving iBCC's aggressive growth and invasive behavior.

To achieve this, we employed mass spectrometry imaging (MSI),[20] which can sensitively detect metabolites in situ while preserving spatial information, enabling detailed analysis of metabolic differences and distribution between and within iBCC samples. By combining single-cell transcriptomics with spatial metabolomics, we highlighted metabolic differences between tumor and normal cells, as well as alterations at the tumor invasive area, providing a detailed depiction of the metabolic microenvironment in eyelid iBCC.

Methods

Ethics Approval

The human clinical study received approval from the Ethics Committee and the Institutional Review Board of Zhongshan Ophthalmic Center, Sun Yat-Sen University (Ethics number: 2024KYPJ012). We adhered to all institutional regulations regarding the ethical use of human volunteer information and samples, and informed consent was obtained from each participant. The human tissue experiments complied with the guidelines of the ARVO Best Practices for Using Human Eye Tissue in Research (Nov2021).

Human Eyelid Basal Cell Carcinoma Samples Collection

Four patients with eyelid iBCC who underwent controlled lesion excision at the Oculoplastic Department of Zhongshan Ophthalmic Center were selected (Table). During surgery, one tumor sample and one normal skin sample were collected from each patient for metabolic analysis.

Inclusion criteria:

1. Age between 40 and 75 years
2. Postoperative pathology-confirmed basal cell carcinoma and confirmed as infiltrative subtype
3. Absence of other underlying metabolic diseases (e.g., diabetes, hyperthyroidism) or cancers before surgery
4. No prior radiotherapy or chemotherapy

Data Sets

The single-cell basal cell carcinoma data were sourced from the GEO database (GSE141526).[17] Raw gene expression profiles of four basal cell carcinoma samples and two normal samples were used.

Copy Variation Analysis for Individual Samples

The copy variation analysis and the identification of the malignant cell and subclone area was conducted by SCEVAN R packages.[21]

Quality Control of Raw Matrix

Cells were retained for analysis if they met the following criteria:

1. 350 < genes/cell <5000
2. Cells with less than 10% mitochondrial gene expression
3. Cells not identified as outliers ($P = 1 \times 10^{-3}$)

Table. Patient Information

Patient ID	Affected Eye	Sex	Age, Y	Histology	Stage*	Tumor Location	Central Ulceration	Recurrent Bleeding	Tumor Size, mm	Disease Onset, Y	Sample Name
635378	OD	Male	69	Infiltrative	Common BCC IIA	Upper eyelid	No	No	10 × 5	6	C1; P1
650633	OS	Male	71	Infiltrative	Common BCC IIA	Upper eyelid	No	No	10 × 4	2	C2
646815	OS	Male	56	Infiltrative	Common BCC IIA	Lower eyelid	Yes	Yes	9 × 5.5	4	C3; P2
643244	OS	Female	57	Infiltrative	Common BCC IIA	Lower eyelid	Yes	Yes	8 × 6	5	C4

* Staging standard follows European Association of Dermato-Oncology classification and staging for BCC.

Investigative Ophthalmology & Visual Science

Data Integration

Following quality control, UMI count matrices were log-normalized and scaled using Seurat. Batch processing and sequencing were conducted. Batch effect correction used the Harmony algorithm (version 1.2.0).[22] Dimensionality reduction, clustering, and differential expression analysis followed Seurat's tutorial, employing principal component analysis (PCA) and Uniform Manifold Approximation and Projection (UMAP) with 20 principal components.

Marker Gene Selection and Clustering

Graph-based clustering was performed using Seurat's "FindClusters" function (clustering resolution = 0.3, k-nearest neighbors = 20). Marker genes for each cluster were identified using the "FindAllMarkers" function, with criteria min.pct > 0.25 and logfc.threshold > 0.25. The top 100 ranked marker genes were selected for each cluster (Supplementary Table S1).

Differential Gene Expression Analysis

Differential gene expression between tumor and normal cells was analyzed using the "FindMarkers" function with the Wilcoxon test. Genes with adjusted |log fold change| > 0.25 and adjusted $P < 0.05$ were considered differentially expressed.

Gene Ontology (GO) Enrichment, Kyoto Encyclopedia of Genes and Genomes, and Gene Set Enrichment Analysis

Functional enrichment analysis of marker and differentially expressed genes was performed using Metascape (https://metascape.org/gp/index.html), visualized with the ggplot2 R package (version 3.3.5). Kyoto Encyclopedia of Genes and Genomes (KEGG) analysis used the clusterProfiler R package (version 4.8.3).

Gene Set Variation Analysis

Gene set variation analysis (GSVA) is an unsupervised analytical method commonly used to assess enrichment scores of samples within predefined gene sets. GSVA compares the enrichment score differences between samples to reveal changes in gene set activity under different conditions or between groups. The GSVA analysis is performed by GSVA R package. The upregulated/downregulated pathways with $P < 0.05$ were considered significant and visualized (Supplementary Fig. S4A). Gene sets for metabolism-related pathways are sourced from the Cancer Cell Metabolism Gene Database (http://bioinfo.uth.edu/),[23] a comprehensive annotation resource focused on cell metabolism genes in cancer. This database provides valuable resources on the functional annotations of cell metabolism genes across various cancer types, supporting research on cancer cell metabolism and broader studies.

Single-Cell Flux Estimation Analysis

Single-cell metabolic flux analysis was conducted using scFEA[24] (v1.1; Python 3.9). Metabolic module data were downloaded from the official website (https://github.com/changwn/scFEA).

Sample Preparation

Postsurgical basal cell carcinoma samples were embedded in optimal cutting temperature (OCT) and stored at −80°C before analysis. Tissues were placed at −20°C 1 hour before use, and tissue sections were prepared using a Leica CM1950 cryostat (Leica Microsystems GmbH, Wetzlar, Germany). Tissue sections of 20 mm thickness were thaw mounted onto ITO-coated microscopic slides (Bruker Daltonics, Billerica, MA, USA) for matrix assisted laser desorption ionization (MALDI) MSI and onto glass slides for hematoxylin and eosin (H&E) staining. The mounted tissue sections were dried for 30 minutes in a desiccator prior to matrix application and then transferred them to a −80°C refrigerator for sealing storage after vacuum packaging.

MALDI Matrix Preparation and Application

In total, 5 mg/mL alpha-cyano-4-hydroxycinnamic acid (CHCA) was dissolved in 70% HPLC-grade Acetonitrile, a solvent frequently used in HPLC (CAN) with 0.1% trifluoroacetic acid (TFA). The 20-µm-thick tissue sections were sprayed using a TM-sprayer (HTX Technologies, Chapel Hill, North Carolina, US). The parameters of the matrix application set in the TM-sprayer were as follows: spray nozzle velocity (1200 mm/min), track spacing (3 mm), flow rate (0.08 mL/min), spray nozzle temperature (60°C), and nitrogen gas pressure (10 psi).

Mass Spectrometry Imaging

Place the conductive slides with the sprayed matrix onto the target plate of the Timstof flex MALDI-2. Using the Bruker Data Imaging software, select the detection area of the tissue sections and set the imaging resolution. The tissue section is divided into several two-dimensional grids based on its size for imaging. At an appropriate laser energy level, the tissue sections are scanned, and the molecules ionized and released from the target sites are detected by mass spectrometry, generating raw data files (Raw Data).

The specific parameters are as follows:

Detection Conditions	Parameter Information
The *m/z* (mass-to-charge ratio) detection range for metabolites	50–1000 *m/z*
Ion detection mode	Negative ion
Spatial resolution (µm)	10
Laser frequency (Hz)	10,000
Laser energy (%)	70
Laser shots per 20 µm pixel (times)	200

Data Analysis

MSI data were analyzed using SCiLS Lab software (version 2021c premium; Bruker Daltonics) with the root mean square normalization. Metabolites were identified by comparing the accuracy of the *m/z* value (<10 ppm) with the in-house database and Bruker Library MS-Metabobase 3.0 database. Receiver operating characteristic analysis and Student's *t*-test analysis were applied to determine the significance of differences between the samples/segmentations. Area under the curve >0.7 or <0.3 and corrected $P < 0.01$ were used to screen significant changed metabolites.

Results

Construction of Single-Cell Transcriptome Atlas for Human Basal Cell Carcinoma

We obtained single-cell RNA sequencing (scRNA-seq) data from the GEO database (GSE141526),[17] including primary human BCC samples ($n = 4$) and peri-tumoral skin (PTS) tissues ($n = 2$). In total, we processed 38,435 raw single cells. Following the removal of doublets and quality control filtering, 38,373 cells were retained for downstream analysis.

To elucidate the cellular diversity and heterogeneity within each tumor and to map the distribution of malignant cells in each sample, we analyzed individual samples using the SCEVAN R package.[21] The results revealed distinct boundaries between tumor and normal cells in BCC1 and BCC2, while BCC3 and BCC4 showed more diffuse boundaries, indicating greater tumor cell invasion and infiltration (Supplementary Fig. S1A). These findings are consistent with the clinical subtypes of the respective samples: BCC1 and BCC2 as nodular BCC and BCC3 and BCC4 as infiltrative BCC.

The copy number variation (CNV) analysis showed varying subclone numbers in the BCC samples (Supplementary Fig. S1B). BCC1 had five subclone regions with an increased copy number on chromosome 6. BCC2 had nine subclone regions with a reduced copy number on chromosomes 11 and 12. BCC3 had four subclone regions with no significant genomic abnormalities. BCC4 had four subclone regions with increased copy numbers on chromosomes 5 and 7.

After integrating BCC samples (BCC1–BCC4) and PTS samples (PTS1–PTS2) (Supplementary Fig. S1C),we clustered the integrated data into a total of 12 subgroups. Based on common tumor biomarkers (Fig. 1B), we identified eight cell types and visualizing them using the UMAP plots, including BCC and PTS (Fig. 1B). The epithelial cell clusters included basal epithelial/tumor cells (KRT14), proliferative epithelial cells (MKI67), and terminally differentiated keratinocytes (IVL). Two types of fibroblasts were identified based on commonly expressed genes in fibroblasts (COL1A1, COL1A2). Among these, cluster 3 and cluster 11 were PDGFRA$^+$ cells, which we defined as inflammatory cancer-associated fibroblasts (iCAFs) based on previous studies.[25] Cluster 5 specifically expressed RGS5, and we termed these cells myofibroblastic cancer-associated fibroblasts (myoCAFs). Other cell types were identified using common marker genes, including endothelial cells (ECs) (PECAM1), melanocytes (MLANA), and immune cells (PTPRC).

Analysis of Fibroblast Subpopulations in Human Basal Cell Carcinoma

Fibroblasts exhibited notable differences between PTS and BCC samples (Fig. 1B). To further investigate these differences, we performed a subpopulation analysis of fibroblasts in the integrated samples. This analysis revealed two distinct fibroblast subtypes: iCAFs, characterized by PDGFRA expression, and myoCAFs, characterized by RGS5 expression. Interestingly, a small number of iCAFs and myoCAFs were also identified in PTS, suggesting potential tumor cell infiltration and invasion.

To elucidate the functions of these two fibroblast subtypes, we analyzed their differentially expressed genes (Supplementary Fig. S2A). Notably, PLA2G2A and CFD were upregulated in iCAFs (Supplementary Fig. S2B). This finding is consistent with previous breast cancer studies that highlighted the unique expression of phospholipase encoded by PLA2G2A and complement pathway-related genes (such as CFD and C3) in iCAFs.[26] GO enrichment analysis of iCAFs (Supplementary Fig. S2C) indicated their involvement in extracellular matrix organization, collagen metabolism regulation, and inflammatory chemotaxis.

In myoCAFs, we observed specific upregulation of RERGL and FHL5 (Supplementary Fig. S2B), both of which are related to angiogenesis.[27] GO analysis (Supplementary Fig. S2C) also showed significant enrichment of myoCAFs in muscle system processes and angiogenesis-related pathways.

These findings suggest that iCAFs and myoCAFs exhibit distinct heterogeneity and may play different roles in the development and progression of BCC. iCAFs appear to be involved in extracellular matrix remodeling, collagen metabolism, and inflammatory processes, while myoCAFs are likely associated with angiogenesis and muscle system processes.

Metabolic Reprogramming in Human Infiltrative Basal Cell Carcinoma

To illustrate the comprehensive metabolic changes in BCC, we first analyzed the GSVA scores of KEGG pathways between BCC and PTS samples (Supplementary Fig. S4A). Overall, multiple metabolic pathways were upregulated in BCC compared to PTS, with the fructose and mannose metabolism pathway showing the most significant difference. Previous studies have shown that fructose enhances the Warburg effect by downregulating mitochondrial respiration and increasing aerobic glycolysis, which may support metastatic cancer growth[28] and drive metabolic reprogramming in cancer cells.[29] In melanoma cells, fructose activates cryoprotection by inducing heme oxygenase 1 expression, helping cells resist immune-mediated killing during immune checkpoint blockade therapy.[30] Other pathways related to lipid and amino acid metabolism also showed notable upregulation.

Given the significant metabolic activation observed in BCC samples, we conducted a detailed analysis of gene set variation in metabolic pathways across all BCC clusters (Supplementary Fig. S4B). This analysis revealed that, in contrast to tumor cells, stromal clusters in BCC (including iCAFs, myoCAFs, ECs, and immune cells) display more pronounced metabolic activity. Based on these findings, we chose to treat tumor cells as a single group in subsequent metabolic pathway analyses to facilitate a comparison of metabolic differences between tumor and stromal tissue and to further explore the specific metabolic module changes and its metabolic flux in different clusters in BCC.

We used the scFEA R package[24] to predict metabolic modules in iBCC subsets (BCC3, BCC4). First, we predicted the tricarboxylic acid cycle (TCA) modules (Figs. 2A, 2B) and found an upregulation of citrate across all clusters. The concentration of citrate in the tumor microenvironment has been reported to be involved in maintaining tumor growth.[31] In vitro experiments have also shown that physiological concentrations of citrate can sustain the proliferation of various cancer cells, including prostate, pancreatic, and gastric cancer cells.[32,33]

We observed a significant upregulation of pyruvate in iCAFs (Fig. 2A), which is consistent with findings from other studies.[34] In primary lymphomas, CAFs were found to

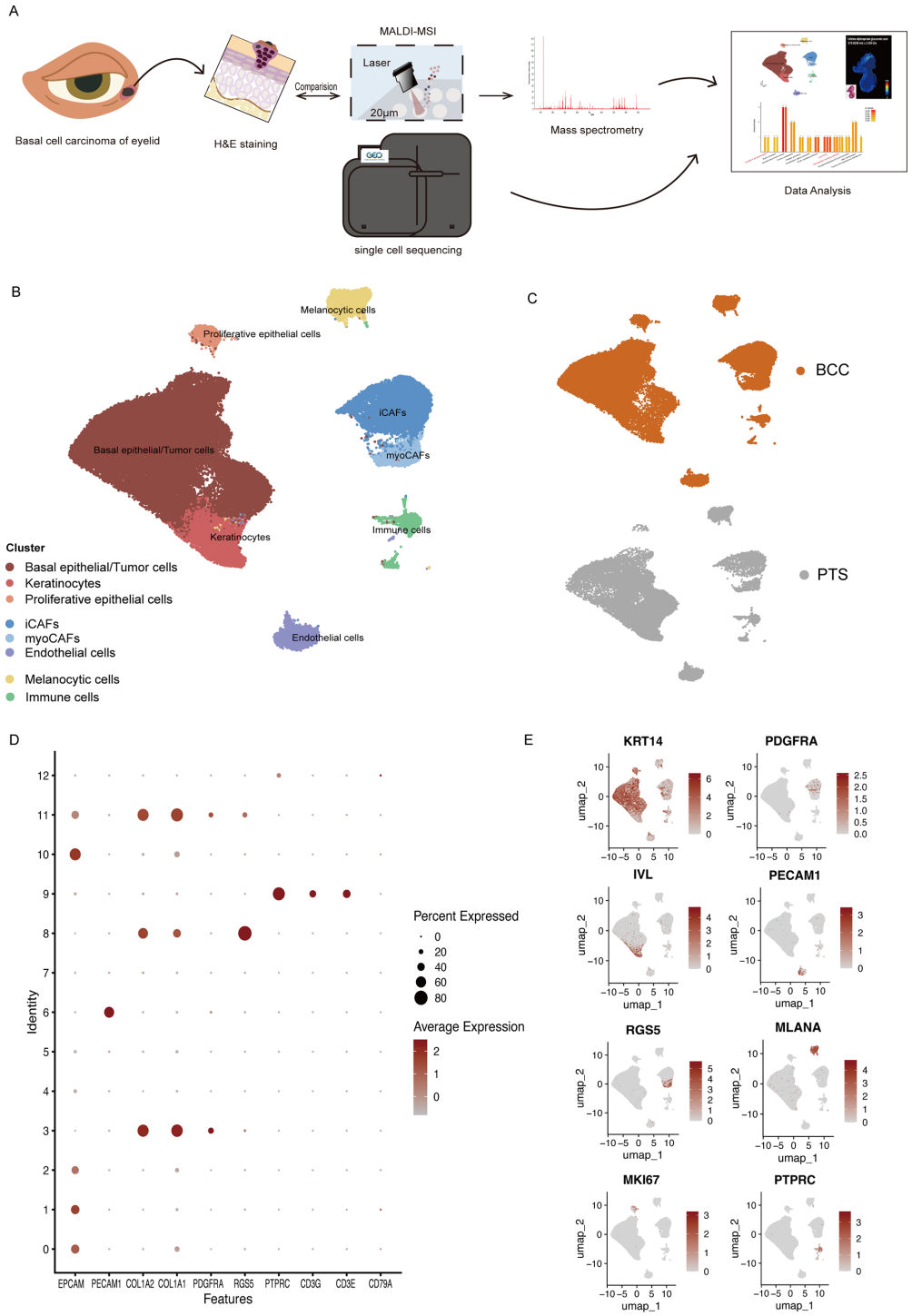

Figure 1. Construction of a single-cell sequencing atlas of human basal cell carcinoma. (**A**) Flowchart of scRNA-seq and MSI analysis of the human basal cell carcinoma. (**B**) UMAP plot displays different cell types in the integrated samples. (**C**) UMAP showing the distribution of cells in BCC and PTS. (**D**) Dotplot showing the common markers of tumor clustering. (**E**) Feature plots display the expression profiles of cell type–specific marker genes for different clusters in human BCC.

secrete significant amounts of pyruvate, and the presence of pyruvate promoted the survival of lymphoma cells. However, we did not observe a significantly high expression of pyruvate in myoCAFs, suggesting that the maintenance of tumor cell survival mainly relies on iCAFs.

Furthermore, we observed a significant upregulation in the first five modules of the TCA, corresponding to the glycolysis process (Fig. 2B). This indicates an increased rate of energy production in tumor cells, which are in a high metabolic state. Notably, this upregulation was also observed in tumor microenvironment–related cell types, including CAFs, ECs, and immune cells. These findings further demonstrate the "nutrient" role of the tumor microenvironment in supporting tumor growth and survival.

Investigative Ophthalmology & Visual Science

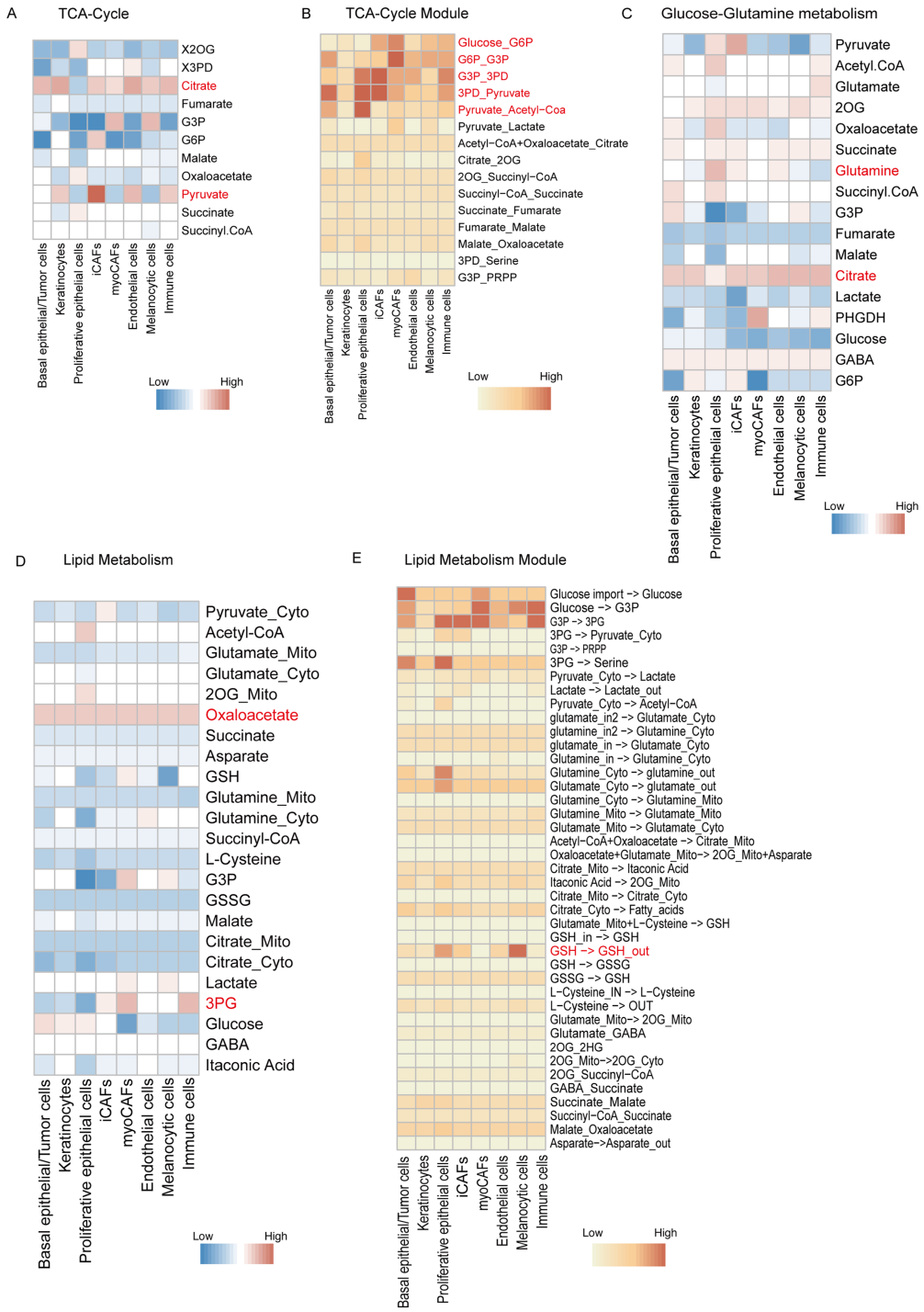

Figure 2. Cellular metabolic flux analysis of human infiltrative basal cell carcinoma. (**A**) Heatmap showing the predicted expression levels of metabolites in the TCA cycle. (**B**) Heatmap showing the metabolic flux of the TCA cycle modules. (**C**) Heatmap showing the predicted expression levels of glucose–glutamine cycle metabolites. (**D**) Heatmap showing the predicted expression levels of metabolites in lipid metabolism. (**E**) Heatmap showing the metabolic fluxes of the lipid metabolism module.

We next analyzed the changes in metabolites in the glucose–glutamine metabolic pathway (Fig. 2C). Interestingly, we observed that the expression of glutamine is higher in proliferative epithelial cells compared to tumor cells. Recent studies have highlighted the importance of glutamine metabolism in maintaining the proliferation and apoptosis of tumor epithelial cells.[35] In tumor cells that use glutamine as a source of energy and building materials, a portion of the TCA cycle shows an opposite direction for reactions from α-ketoglutarate to isocitrate. In this manner, α-ketoglutarate, which originates from glutaminolysis, supplies the TCA cycle in the opposite direction,[36] potentially contributing to the accumulation of citrate (Fig. 2C). Furthermore, an increase in phosphoglycerate dehydrogenase (PHGDH) was

Investigative Ophthalmology & Visual Science

observed in both myoCAFs and immune cells, suggesting the importance of these cell types in supporting tumor metabolism.

Given that BCC is highly associated with DNA damage caused by photodamage, we investigated the metabolic changes in the methionine–glutathione–folate network (Supplementary Fig. S2D) to assess DNA methylation and related metabolic alterations. Ultraviolet radiation induces carcinogenic photoproducts such as cyclobutane pyrimidine dimers and 6-4 pyrimidone photoproducts, leading to DNA mutations and local immunosuppression.[37] Compared to other cells, we found an increase in S-adenosylmethionine and 5,10-methylenetetrahydrofolate in immune cells. Recent literature also reports that DNA methylation is related to metabolic remodeling in immune cells within the tumor microenvironment,[38] highlighting the complex interplay between epigenetic regulation and metabolism in the immune compartment of iBCC.

In the iron-related metabolism (Supplementary Fig. S2E), we observed high expression of heme and heme-associated metabolites in both tumor cells and proliferative epithelial cells, along with a mild upregulation of these metabolites in the cell components of the tumor microenvironment (ECs, CAFs, and immune cells). Heme was known to be an important factor in the tumor microenvironment and was involved in macrophage polarization, angiogenic potential of tumor endothelial cells, matrix remodeling by cancer-associated fibroblasts, and interactions between neural and cancer cells.[39] The significance of these substances in the tumor microenvironment is noteworthy and will be further elucidated in the upcoming spatial metabolomics analysis.

Our analysis of the metabolic changes in the tumor microenvironment of iBCC revealed significant alterations in lipid metabolism (Fig. 2E).[40] Notably, we observed a substantial increase in oxaloacetate levels across all cell subgroups. Oxaloacetate has been implicated in nucleotide biosynthesis in rapidly proliferating cancer cells and plays a pivotal role in metabolic reprogramming in various cancer models.[41]

In addition to oxaloacetate, we found an upregulation of 3-phosphoglycerate (3PG) in immune cells and CAF cell types. Concurrently, a significant increase in the metabolic flux of the 3PG → serine pathway was observed in cancer cells and proliferative epithelial cancer cells (Fig. 2E). Previous studies suggested that the glycolysis intermediate 3PG can be diverted to produce serine, and during solid tumor progression, the stiffness of the extracellular matrix in the tumor microenvironment may enhance glycolysis-derived serine biosynthesis.[42] As CAFs are closely associated with tumor extracellular matrix reprogramming, they may further influence tumor serine biosynthesis by upregulating 3PG, thereby regulating tumor growth and invasion.

We also observed an increase in glutathione (GSH) metabolic flux in ECs, iCAFs, melanocytes, and proliferative ECs (Fig. 2E). In human squamous cell carcinoma, CAFs have been shown to utilize glutamate to form glutathione, balancing cellular redox status and promoting stromal extracellular matrix remodeling.[43] Furthermore, a significant upregulation of glutathione was also found in melanocytes, which may be due to UVA-mediated melanogenesis caused by excessive production of oxidants and deterioration of the antioxidant defense network.[44]

Our results demonstrate that the iBCC microenvironment exhibits enhanced metabolic flux in glycolysis, glutamine, heme, and glutathione pathways. Moreover, we observed significant differences in the metabolic profiles of the two types of CAFs. In iCAFs, pyruvate content was relatively high, while in myoCAFs, PHGDH and 3PG were highly expressed, indicating their function in extracellular matrix reprogramming.

MALDI MSI Reveals Metabolic Complexity in Human Infiltrative Basal Cell Carcinoma of the Eyelid

To corroborate the metabolic alterations in iBCC identified through single-cell analysis and to elucidate the complex metabolic landscape of the tumor microenvironment, we collected four samples for MALDI MSI (Table; Methods; Fig. 1A). Due to the specificity of tumor resection surgery, some sections were able to display changes in the tumor invasive zone (Fig. 3A). Both tumor and stroma regions were identified in the samples (Fig. 3B). Compared with H&E staining, red pixels exhibited spatial characteristics similar to stroma regions, while the spatial distribution of yellow pixels was consistent with tumor regions (Fig. 3C).

We identified metabolic similarities in the MS images of each BCC sample using bipartitional k-means clustering, which grouped image pixels with similar metabolic fingerprints together.[45] Both C1 and C2 were divided into six clusters, suggesting a high degree of metabolic complexity within the tumor (Fig. 3D). Further analysis revealed that all detected features could be separated into six major components (Supplementary Fig. S3A).

We detected numerous active components in human eyelid iBCC samples (Figs. 3E, 3F). The top 10 categories of substances included carboxylic acids and their derivatives, aromatic hydrocarbons, fatty acyls, steroids, and glycerophospholipids. The significant presence of metabolites related to lipid metabolism suggested a high degree of lipid metabolic heterogeneity in iBCC.

We analyzed the metabolites that were upregulated in all iBCC samples compared to normal skin (Fig. 4A). Taurine showed a significant increase in all four tumor samples (Fig. 4B). Previous studies have shown elevated levels of taurine in primitive embryonic tumors[46] and brain tumors such as retinoblastoma, medulloblastoma, and neuroblastoma.[47,48] Deoxy-GMP, associated with DNA damage caused by light exposure, a significant pathogenic factor in BCC, was also upregulated. This suggests its role as an activated carcinogenic metabolite that binds to DNA and forms adducts, inducing gene mutations and accelerating tumor progression[49] (Fig. 4C). O-Phosphoethanolamine, significantly elevated in tumors (Fig. 4D), is linked to tumor growth, endurance in harsh microenvironments, invasion, and infiltration.[50] Pyrithione, a heat shock response inducer causing DNA damage and impaired genomic integrity, was also upregulated.[51]

Notably, metabolites associated with carbohydrate metabolism (such as ATP, UTP, and sodium lactate) are upregulated in samples C3 and C4 compared to C1 and C2 (Fig. 4A). This may be due to the presence of central ulceration and recurrent bleeding in the C3 and C4 samples, making them more aggressive compared to the C1 and C2 samples and thereby requiring more rapid energy support.

KEGG enrichment analysis revealed that the sphingolipid signaling pathway, with O-phosphoethanolamine as a key

Investigative Ophthalmology & Visual Science

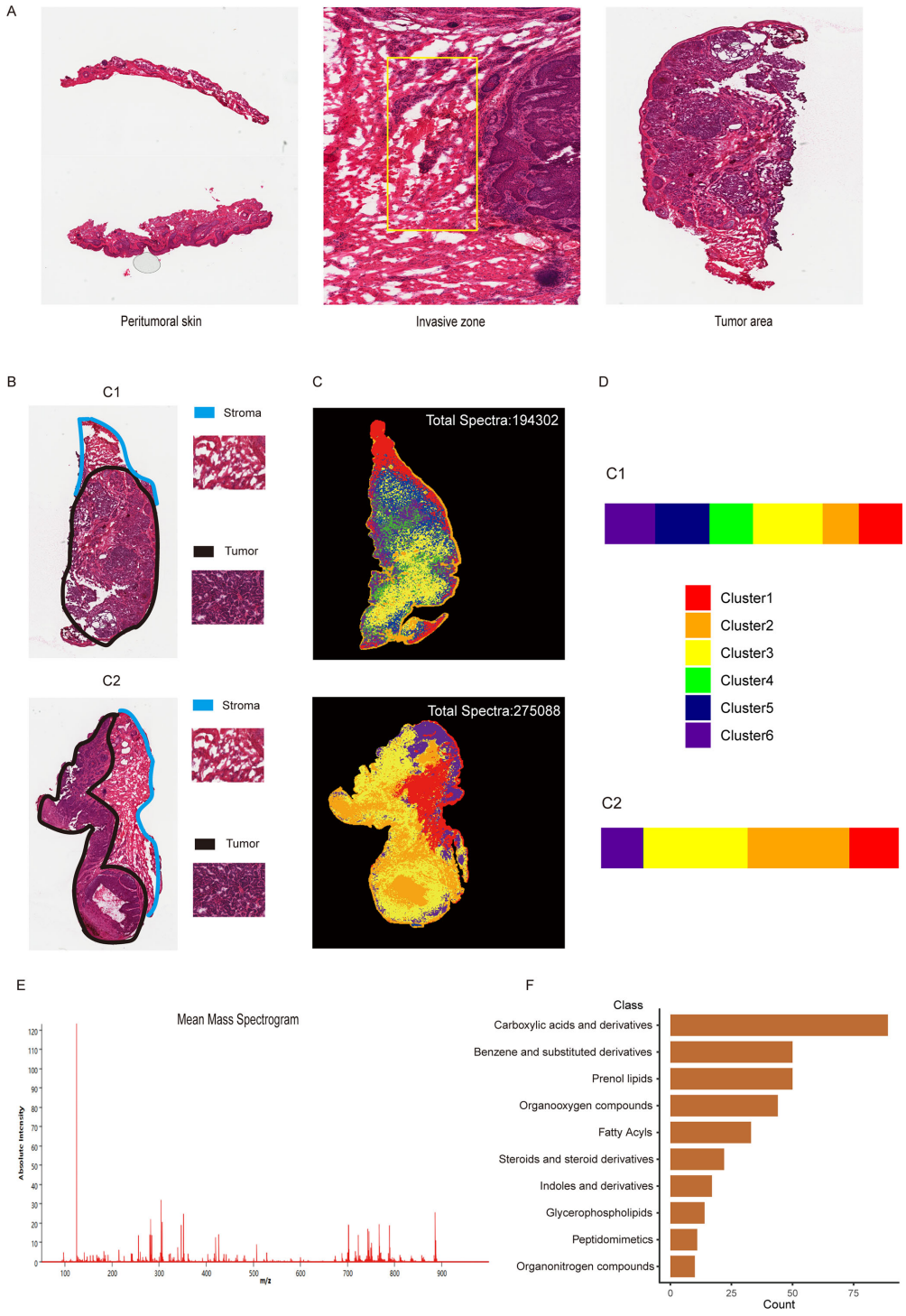

Figure 3. Construction of spatial metabolic landscape of human eyelid infiltrative basal cell carcinoma. (**A**) H&E staining of basal cell carcinoma tumor area, invasive zone, and peritumoral area. (**B**) H&E staining of basal cell carcinoma sample where *blue areas* represent stroma regions, and *black areas* represent tumor regions. (**C**) Sample pixel clustering analysis (k-means); both samples are divided into six clusters. (**D**) Metabolite clustering proportions of C1 and C2 samples. (**E**) Average mass spectrum of metabolites in basal cell carcinoma samples, with mass-to-charge ratio on the x-axis and peak intensity information on the y-axis. (**F**) Barplot displays the top 10 detected types of metabolites in samples.

metabolite, was upregulated in all four tumor samples (Supplementary Fig. S3B). O-phosphoethanolamine, derived from sphingosine-1-phosphate (S1P), is linked to cancer cell transformation, migration, growth, and resistance.[52] In C1, C3, and C4, the lysosomal metabolism pathway was upregulated, likely due to the high carbohydrate affinity required by rapidly proliferating cancer cells.[53]

We then investigated the downregulated metabolites in four iBCC samples (Fig. 4F). Conjugated linoleic acid (Fig. 4G), known for its antitumor effects

Investigative Ophthalmology & Visual Science

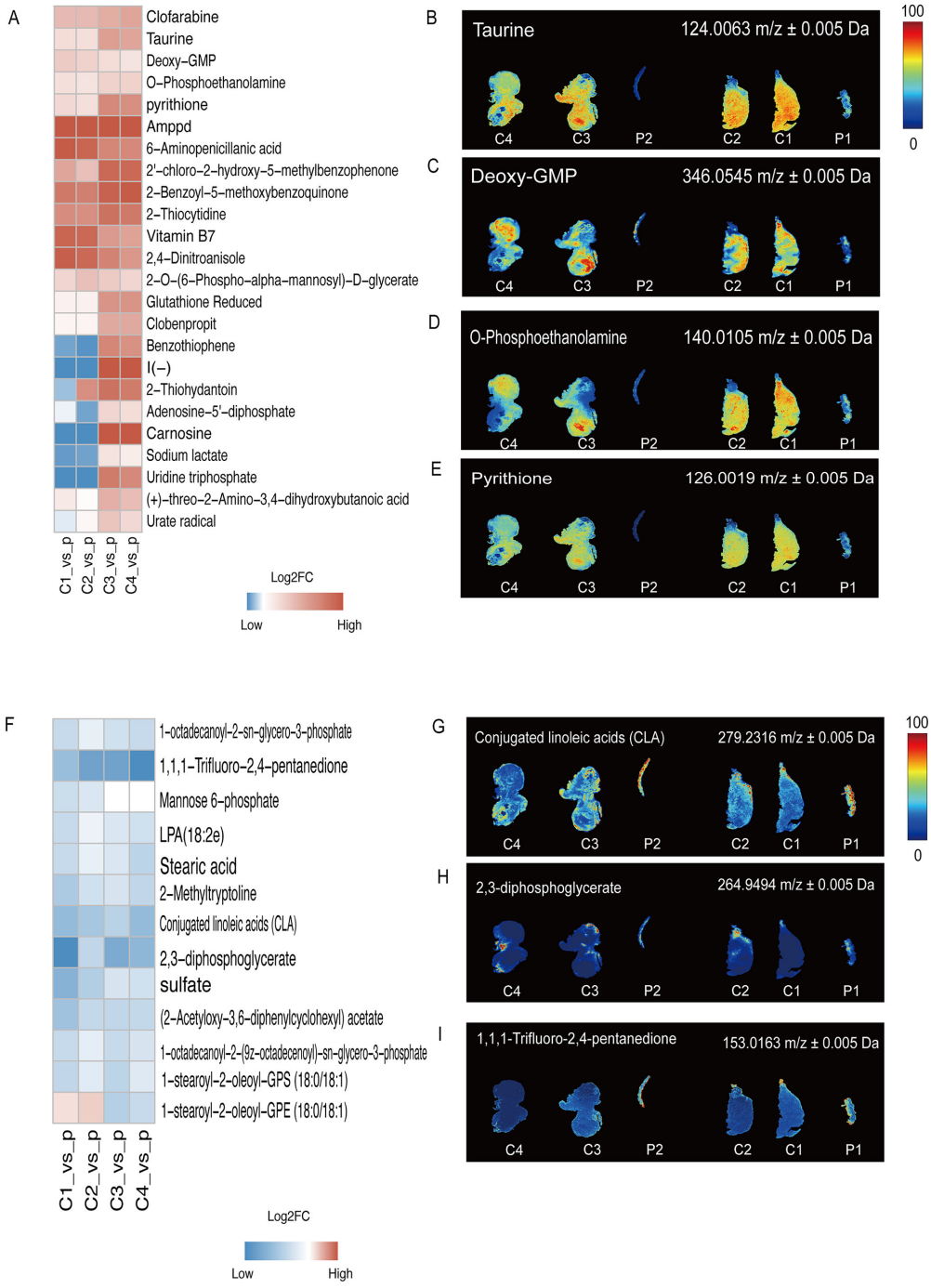

Figure 4. Differential metabolite analysis in human eyelid infiltrative basal cell carcinoma. **(A)** Heatmap showing the upregulation of metabolite in different BCC samples. Metabolites with an area under the curve (AUC) >0.7 and a corrected $P < 0.01$ were considered significantly upregulated. The four metabolites with the highest AUC values in the receiver operating characteristic (ROC) curve are displayed in **Bcu**. **(B)** Mass spectrometry image of taurine. **(C)** Mass spectrometry image of deoxy-GMP. **(D)** Mass spectrometry image of O-phosphoethanolamine. **(E)** Mass spectrometry image of pyrithione. **(F)** Heatmap showing the downregulation of metabolite in different BCC samples. Metabolites with an AUC <0.3 and a corrected $P < 0.01$ were considered significantly downregulated. The three metabolites with the highest AUC values in the ROC curve are displayed in **Ghe**. (G) Mass spectrometry images of conjugated linoleic acid. **(H)** Mass spectrometry images of 2,3-diphosphoglycerate. **(I)** Mass spectrometry images of 1,1,1-trifluoro-2,4-pentanedione.

in skin keratinocytes, was significantly reduced in all four samples.[54] Compared to normal skin, 2,3-bisphosphoglycerate (Fig. 4H) was significantly downregulated, indicating enhanced glycolysis in tumor tissues, consistent with previous literature and our findings.[55,56]

Metabolite Similarity and Differences Between Tumor and Invasive Zone in iBCC

Since iBCC strongly interacts with its nearby environment, we subdivided the slice into microregions to analyze the

Investigative Ophthalmology & Visual Science

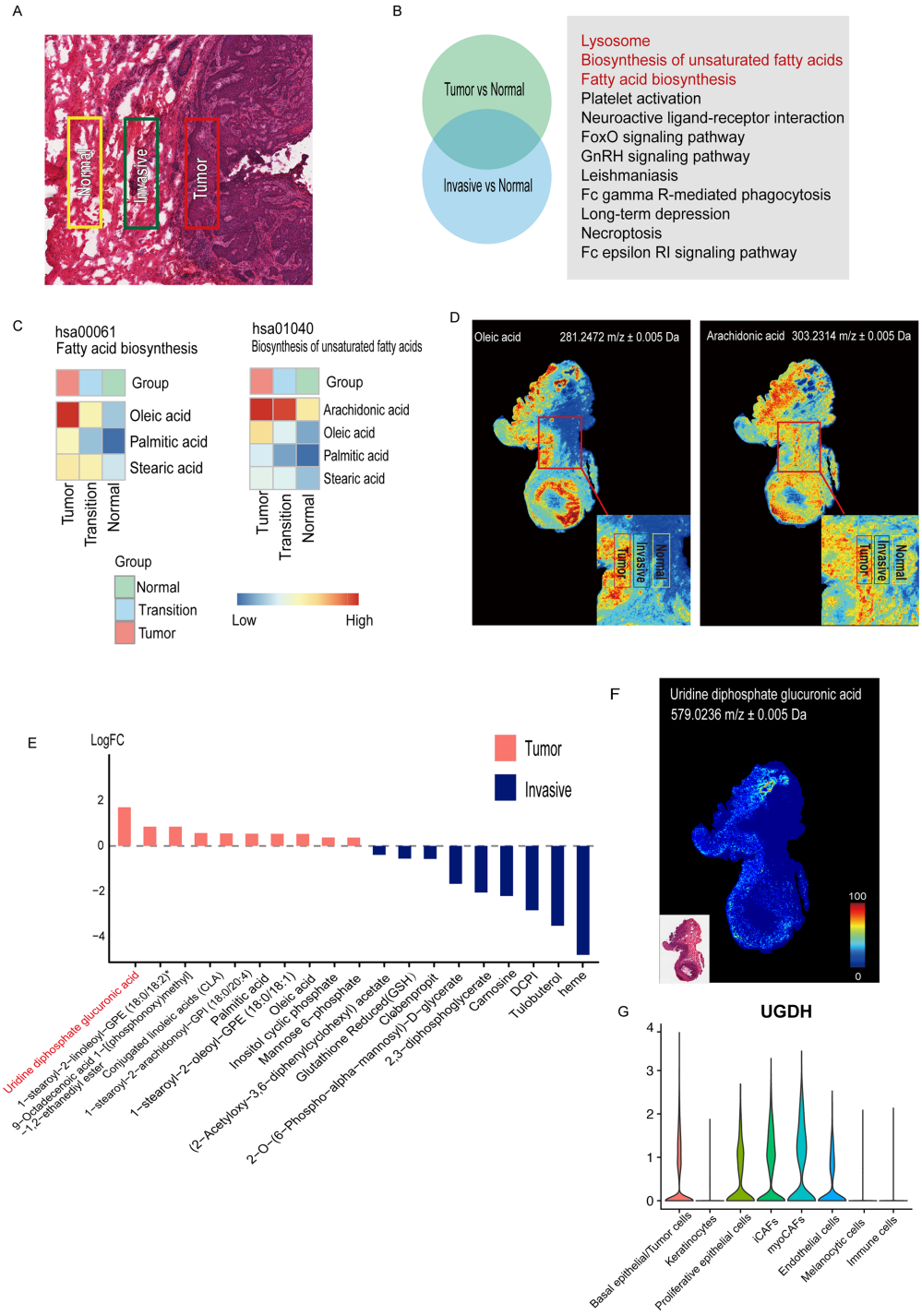

Figure 5. Metabolic changes of the invasive area of human basal cell carcinoma. (**A**) H&E staining of tumor area, tumor invasive area, and normal area. (**B**) The share enriched KEGG pathways between tumor and invasive area ($P < 0.05$). (**C**) Heatmap showing the metabolites enriched in pathways hsa00061 and hsa01040 and their expression levels in tumor, invasive, and normal areas. (**D**) Mass spectrometry images of oleic acid and arachidonic acid; the schematic diagram in the *lower right corner* shows the enlarged view of the tumor, invasive area, and normal area. (**E**) Barplot showing the differentially upregulated metabolites in tumor and invasive regions. Differences between the tumor area and invasive zone with AUC >0.7 or <0.3 and corrected $P < 0.01$ were considered significant upregulated/downregulated metabolites. (**F**) Metabolic mass spectrometry image of UDPGA. (**G**) Violin plot showing the distribution of UDP-glucose 6-dehydrogenase (UGDH) in various clusters in BCC samples.

tumor–stroma interactions at the invasive zone.[57] The locations of tumor, invasive zone, and normal area in iBCC were identified (Fig. 5A).

KEGG enrichment analysis showed that lipid metabolism–related pathways were upregulated in both the tumor and invasive area compared to normal tissue (Fig. 5B). In the fatty acid biosynthesis pathway (hsa00061), oleic acid was found to be highly expressed in the invasive area (Figs. 5C, 5D). CAFs in xenograft tumors have been reported to contain higher levels of oleic acid, which can activate lipid metabolism in cancer cells under glucose deprivation conditions, enhancing their stem cell activity

Investigative Ophthalmology & Visual Science

and contributing to malignant progression.[58] Additionally, in the biosynthesis pathway of unsaturated fatty acids (hsa01040), arachidonic acid was highly expressed in both the tumor and invasive area (Figs. 5C, 5D). As an important mediator of inflammation, arachidonic acid is closely related to the maintenance of chronic inflammation in the tumor microenvironment and the immune infiltration of tumor-associated immune cells.[59] These findings underscore the significant impact of lipid metabolism in the tumor microenvironment on BCC proliferation and immune suppression.

We also investigated the metabolic differences between the tumor and invasive zone (Fig. 5E). GSH levels were higher in the invasive area, consistent with our previous single-cell findings (Fig. 2E). In human skin squamous cell carcinoma, CAFs use glutamate to form glutathione, balancing cellular redox states and promoting extracellular matrix remodeling.[60] Furthermore, glutathione levels increase by 30% in prostate cancer cells grown in CAF-conditioned media,[61] suggesting that elevated GSH in tumor cells may result from CAF regulation.

Heme levels were significantly higher in the invasive zone compared to the tumor area. This finding aligns with recent literature indicating that heme can modulate the tumor microenvironment by acting on tumor-associated endothelial cells and tumor-associated macrophages, promoting angiogenesis and tumor immune suppression, in addition to supporting cancer cell growth, survival, and metastasis.[62] Elevated levels of carnosine were also found in the invasive zone.

UXS1 as a Potential Target to Counteract Drug Resistance in Basal Cell Carcinoma

Among the upregulated metabolites in the tumor area, UDP-glucuronic acid (UDPGA) exhibited the highest expression (Figs. 5E, 5F). UDPGA plays a crucial role in glycosylation within the Golgi apparatus and serves as a key substrate for UDP-glucuronosyltransferase (UGTs).[63] These enzymes utilize UDPGA to conjugate glucuronic acid to xenobiotics, including chemotherapy drugs, facilitating their deactivation and secretion through glucuronidation. This process may contribute to tumor drug resistance.[64]

Recent research has highlighted the potential of UXS1 as a regulatory point, as it can convert UDPGA to UDP-xylose, thereby reducing UDPGA accumulation. However, this effect is only observed in tumors with high UDP-glucose 6-dehydrogenase (UGDH) expression.[65] In non–small cell lung cancer with high UGDH expression, the induction of UXS1 loss significantly slows tumor growth and extends the median survival time for chemotherapy drugs A549 and H460.[65,66]

Motivated by these findings, we explored whether BCC exhibits high UDPH expression. We examined the distribution of UGDH (Fig. 5G) and found high expression levels in tumor cells and tumor microenvironment cells, including myoCAFs, iCAFs, and ECs. The elevated expression of UGDH in both tumor cells and stromal cells suggests active remodelling of the ECM within the BCC microenvironment, potentially contributing to tumor progression and invasion.

Discussion

Infiltrative basal cell carcinoma of the eyelid is a highly aggressive subtype, presenting substantial challenges due to its invasive growth pattern,[8–10] high risk of recurrence,[13] and considerable treatment burden.[67] Some of the infiltrative cases are considered "difficult to treat" and may need alternative therapies like hedgehog pathway inhibitors (e.g., vismodegib or sonidegib) and immune checkpoint inhibitors (e.g., PD-1), which are approximately 10 times higher than the surgery prices.[16] Our study provides novel insights into the metabolic landscape of this tumor using spatial metabolomics imaging and scRNA-seq. By integrating these advanced techniques, we have mapped the metabolic alterations in the tumor microenvironment and identified potential diagnostic markers and therapeutic targets.

Cellular Metabolic Flux in iBCC

GSVA analysis between BCC and PTS has demonstrated the activation of various metabolic pathways in BCC. The fructose and mannose metabolism pathway showed the most significantly difference between BCC and PTS. Previous studies have demonstrated that fructose enhances the Warburg effect by downregulating mitochondrial respiration and increasing aerobic glycolysis, potentially supporting metastatic cancer growth[28] and driving metabolic reprogramming in cancer cells.[29] Also, there are some pathways related to lipid metabolism and amino acid metabolism, which led us to further explore the metabolic changes and their metabolic flux in different clusters in BCC. For the subsequent metabolic pathway analysis, we opted to consider tumor cells as a whole since gene set variation analysis of metabolic pathways across all BCC clusters revealed that stromal clusters—such as iCAFs, myoCAFs, ECs, and immune cells—undergo more significant metabolic changes than the tumor cells themselves. This suggests that the stroma plays a more dynamic and active role in the metabolic reprogramming of BCC, offering crucial insights into the broader tumor microenvironment and potentially guiding therapeutic strategies that target stromal elements in addition to tumor cells. We investigated the cellular metabolic flux in iBCC, revealing a significant upregulation of glycolytic flux across all clusters within the iBCC microenvironment. This finding is consistent with the high metabolic state of iBCC and highlights the critical role of glycolysis in tumor growth and progression.[55] Notably, elevated glutamine levels were observed in proliferative epithelial cells, suggesting that glutamine plays a crucial role in sustaining the proliferation and apoptosis of tumor epithelial cells.

Metabolic Alterations in the Tumor Microenvironment

Spatial metabolomics imaging allowed us to analyze the metabolic differences between tumor cells and normal cells, as well as the metabolic changes in the tumor invasive area. We identified several metabolites, including taurine, deoxy-GMP, O-phosphoethanolamine, and pyrithione, that were highly expressed across tumor samples, indicating their potential as diagnostic markers for eyelid iBCC. Previous studies on BCC indicated that tumors respond to sudden bursts of fibroblast-specific inflammatory signaling pathways by producing heat shock proteins.[17] The upregulation of pyrithione suggests that the heat shock response in BCC may be induced by pyrithione. The upregulation of the sphingolipid signaling pathway, particularly O-phosphoethanolamine derived from S1P cleavage, highlights

Investigative Ophthalmology & Visual Science

its significance in promoting cancer cell transformation, migration, growth, and drug resistance. Interestingly, we observed that tumors located in the lower eyelids tend to exhibit central ulceration and recurrent bleeding. Additionally, metabolites associated with carbohydrate metabolism, such as ATP, UTP, and sodium lactate, were upregulated in the C3 and C4 samples compared to the C1 and C2 samples. This observation may be attributed to the more aggressive nature of the C3 and C4 samples, likely due to the presence of central ulceration and recurrent bleeding, which demand higher metabolic activity and rapid energy support to sustain the tumor's growth and survival. These findings align with the notion that ulceration and ongoing tissue damage in tumors trigger increased glycolytic and energy demands to support invasive and proliferative cellular activities.[68]

Lipid Metabolism and Lysosomal Pathway Upregulation

Tumor and invasive areas showed upregulation of lipid metabolism pathways, with high expression of oleic and arachidonic acids. This suggests that CAF-derived oleic acid may be transferred to cancer cells for energy production, similar to mechanisms observed in lung adenocarcinoma.[58] The activation of the arachidonic acid pathway in iCAFs and myoCAFs supports their role in maintaining inflammation in the invasive area. The lysosome pathway was also upregulated in both tumor and invasive areas, suggesting that lysosome-induced tumor immunity might also be present in iBCC.

Potential Therapeutic Target

In the tumor area, we observed a specific upregulation of UDPGA. To investigate the potential activation of its upstream gene, we examined UGDH expression in single cells. We found that UGDH was highly expressed in tumor cells, proliferative epithelial cells, iCAFs, myoCAFs, and ECs. UXS1 was only active in tumor cells with high UGDH expression. Given the high expression of UGDH in iBCC, we speculate that UXS1 could also serve as a potential therapeutic target to control tumor proliferation and drug resistance in iBCC.

Limitations of the Study

Despite these findings, our study has several limitations. First, the small sample size, due to difficulties in presurgical tumor type identification, potentially limits the comprehensive understanding of metabolic heterogeneity and spatial diversity. Also, due to the rarity of locally advanced basal cell carcinoma[69] and metastatic basal cell carcinoma,[70] we were unable to collect sufficient samples to present the metabolic changes in different stages iBCC. Second, the analysis of epithelial cell subgroups is insufficient. Additionally, the analysis of interactions between tumor cells and other microenvironment components is limited. Lastly, current MSI methods prevent the capture of cell-specific characteristics and correlations in tissues, thereby limiting metabolomic insights at the single-cell level.

Conclusions

In conclusion, our study provides novel insights into the metabolic landscape of iBCC of the eyelid, revealing the pivotal role of metabolic reprogramming—particularly within stromal cells—in tumor progression. We have identified potential diagnostic markers and therapeutic targets, especially UXS1, and highlighted the complex interplay between metabolic alterations and immune evasion in this aggressive eyelid malignancy. Future research is necessary to further validate these findings and explore clinical applications, such as combination therapies targeting both the tumor and stromal components or investigating the molecular mechanisms driving metabolic shifts in BCC. These efforts may help refine current treatment strategies and ultimately enhance patient outcomes.

Acknowledgments

Supported by the State Key Laboratory of Ophthalmology, Zhongshan Ophthalmic Center, Sun Yat-Sen University. The funding body had no role in study design, collection, management, analysis and interpretation of data, writing of the manuscript, and the decision to submit the manuscript for publication. The spatial metabolomics imaging services were provided by APTBIO Co., Ltd.

Disclosure: **Y. Huang**, None; **C. He**, None; **Q. Hu**, None; **Z. Liu**, None; **X. Li**, None; **W. Gao**, None; **X. Liang**, None; **R. Chen**, None; **Z. Mao**, None; **X. Lin**, None

References

1. Cook BE, Bartley GB. Epidemiologic characteristics and clinical course of patients with malignant eyelid tumors in an incidence cohort in Olmsted County, Minnesota. *Ophthalmology*. 1999;106(4):746–750.
2. Rigel DS, Friedman RJ, Kopf AW. Lifetime risk for development of skin cancer in the U.S. population: current estimate is now 1 in 5. *J Am Acad Dermatol*. 1996;35(6):1012–1013.
3. Oh CC, Jin A, Koh W-P. Trends of cutaneous basal cell carcinoma, squamous cell carcinoma, and melanoma among the Chinese, Malays, and Indians in Singapore from 1968–2016. *JAAD Int*. 2021;4:39–45.
4. de Vries E, Louwman M, Bastiaens M, de Gruijl F, Coebergh JW. Rapid and continuous increases in incidence rates of basal cell carcinoma in the southeast Netherlands since 1973. *J Invest Dermatol*. 2004;123(4):634–638.
5. Flohil SC, Seubring I, van Rossum MM, et al. Trends in Basal cell carcinoma incidence rates: a 37-year Dutch observational study. *J Invest Dermatol*. 2013;133(4):913–918.
6. Peris K, Fargnoli MC, Kaufmann R, et al. European consensus-based interdisciplinary guideline for diagnosis and treatment of basal cell carcinoma—update 2023. *Eur J Cancer*. 2023;192:113254.
7. Scrivener Y, Grosshans E, Cribier B. Variations of basal cell carcinomas according to gender, age, location and histopathological subtype. *Br J Dermatol*. 2002;147(1):41–47.
8. Leibovitch I, McNab A, Sullivan T, Davis G, Selva D. Orbital invasion by periocular basal cell carcinoma. *Ophthalmology*. 2005;112(4):717–723.
9. Mechel E, Tran AQ, North VS, Kazim M. Corneal invasion by basal cell carcinoma. *Ophthalmic Plastic Reconstruct Surg*. 2022;38(2):e63.
10. Sun MT, Wu A, Figueira E, Huilgol S, Selva D. Management of periorbital basal cell carcinoma with orbital invasion. *Future Oncol*. 2015;11(22):3003–3010.
11. Hernandez LE, Mohsin N, Levin N, et al. Basal cell carcinoma: an updated review of pathogenesis and treatment options. *Dermatol Ther*. 2022;35(6):e15501.

12. Rogers HW, Coldiron BM. A relative value unit-based cost comparison of treatment modalities for nonmelanoma skin cancer: effect of the loss of the Mohs multiple surgery reduction exemption. *J Am Acad Dermatol*. 2009;61(1):96–103.
13. Allali J, D'Hermies F, Renard G. Basal cell carcinomas of the eyelids. *Ophthalmologica*. 2005;219(2):57–71.
14. Basset-Seguin N, Sharpe HJ, de Sauvage FJ. Efficacy of Hedgehog pathway inhibitors in basal cell carcinoma. *Mol Cancer Ther*. 2015;14(3):633–641.
15. Guo Y, Rokohl AC, Kopecky A, Heindl LM. Periocular basal cell carcinoma—current treatment concepts. *Ann Eye Sci*. 2021;6:18.
16. Hoorens I, Van Coile L, Jacobs C, et al. Systemic treatment of advanced basal cell carcinoma: how to critically evaluate value for patient and society? *Ther Adv Med Oncol*. 2022;14:17588359221141762.
17. Guerrero-Juarez CF, Lee GH, Liu Y, et al. Single-cell analysis of human basal cell carcinoma reveals novel regulators of tumor growth and the tumor microenvironment. *Sci Adv*. 2022;8(23):eabm7981.
18. Huang L, Wang X, Pei S, et al. Single-cell profiling reveals sustained immune infiltration, surveillance, and tumor heterogeneity in infiltrative basal cell carcinoma. *J Invest Dermatol*. 2023;143(11):2283–2294.
19. Huang J, Schaefer J, Wang Y, et al. Metabolic signature of eyelid basal cell carcinoma. *Exp Eye Res*. 2020;198:108140.
20. Buchberger AR, DeLaney K, Johnson J, Li L. Mass spectrometry imaging: a review of emerging advancements and future insights. *Anal Chem*. 2018;90(1):240–265.
21. De Falco A, Caruso F, Su X-D, Iavarone A, Ceccarelli M. A variational algorithm to detect the clonal copy number substructure of tumors from scRNA-seq data. *Nat Commun*. 2023;14(1):1074.
22. Korsunsky I, Millard N, Fan J, et al. Fast, sensitive and accurate integration of single-cell data with Harmony. *Nat Methods*. 2019;16(12):1289–1296.
23. Kim P, Cheng F, Zhao J, Zhao Z. ccmGDB: a database for cancer cell metabolism genes. *Nucleic Acids Res*. 2016;44(D1):D959–D968.
24. Alghamdi N, Chang W, Dang P, et al. A graph neural network model to estimate cell-wise metabolic flux using single-cell RNA-seq data. *Genome Res*. 2021;31(10):1867–1884.
25. Chen Z, Zhou L, Liu L, et al. Single-cell RNA sequencing highlights the role of inflammatory cancer-associated fibroblasts in bladder urothelial carcinoma. *Nat Commun*. 2020;11(1):5077.
26. Cords L, Tietscher S, Anzeneder T, et al. Cancer-associated fibroblast classification in single-cell and spatial proteomics data. *Nat Commun*. 2023;14(1):4294.
27. Wong D, Auguste G, Lino Cardenas CL, et al. FHL5 controls vascular disease-associated gene programs in smooth muscle cells. *Circ Res*. 2023;132(9):1144–1161.
28. Nakagawa T, Lanaspa MA, Millan IS, et al. Fructose contributes to the Warburg effect for cancer growth. *Cancer Metab*. 2020;8:16.
29. Ting KKY. Fructose-induced metabolic reprogramming of cancer cells. *Front Immunol*. 2024;15:1375461.
30. Kuehm LM, Khojandi N, Piening A, et al. Fructose promotes cytoprotection in melanoma tumors and resistance to immunotherapy. *Cancer Immunol Res*. 2021;9(2):227–238.
31. Icard P, Coquerel A, Wu Z, et al. Understanding the central role of citrate in the metabolism of cancer cells and tumors: an update. *Int J Mol Sci*. 2021;22(12).
32. Mycielska ME, Dettmer K, Rümmele P, et al. Extracellular citrate affects critical elements of cancer cell metabolism and supports cancer development in vivo. *Cancer Res*. 2018;78(10):2513–2523.
33. Haferkamp S, Drexler K, Federlin M, et al. Extracellular citrate fuels cancer cell metabolism and growth. *Front Cell Dev Biol*. 2020;8:602476.
34. Sakamoto A, Kunou S, Shimada K, et al. Pyruvate secreted from patient-derived cancer-associated fibroblasts supports survival of primary lymphoma cells. *Cancer Sci*. 2019;110(1):269–278.
35. Jin J, Byun J-K, Choi Y-K, Park K-G. Targeting glutamine metabolism as a therapeutic strategy for cancer. *Exp Mol Med*. 2023;55(4):706–715.
36. Baryła M, Semeniuk-Wojtaś A, Róg L, et al. Oncometabolites—a link between cancer cells and tumor microenvironment. *Biology*. 2022;11(2).
37. Sullivan TJ. Topical therapies for periorbital cutaneous malignancies: indications and treatment regimens. *Curr Opin Ophthalmol*. 2012;23(5):439–442.
38. Zhong F, Lin Y, Zhao L, et al. Reshaping the tumour immune microenvironment in solid tumours via tumour cell and immune cell DNA methylation: from mechanisms to therapeutics. *Br J Cancer*. 2023;129(1):24–37.
39. Fiorito V, Chiabrando D, Petrillo S, Bertino F, Tolosano E. The multifaceted role of heme in cancer. *Front Oncol*. 2019;9:1540.
40. Anghaei S, Kamyab-Hesari K, Haddadi S, Jolehar M. New diagnostic markers in basal cell carcinoma. *J Oral Maxillofac Pathol*. 2020;24(1):99–105.
41. Chen G, Bao B, Cheng Y, et al. Acetyl-CoA metabolism as a therapeutic target for cancer. *Biomed Pharmacother*. 2023;168:115741.
42. Shunxi W, Xiaoxue Y, Guanbin S, et al. Serine metabolic reprogramming in tumorigenesis, tumor immunity, and clinical treatment. *Adv Nutr*. 2023;14(5):1050–1066.
43. Li Z, Sun C, Qin Z. Metabolic reprogramming of cancer-associated fibroblasts and its effect on cancer cell reprogramming. *Theranostics*. 2021;11(17):8322–8336.
44. Panich U, Onkoksoong T, Limsaengurai S, Akarasereenont P, Wongkajornsilp A. UVA-induced melanogenesis and modulation of glutathione redox system in different melanoma cell lines: the protective effect of gallic acid. *J Photochem Photobiol B Biol*. 2012;108:16–22.
45. Sun C, Liu W, Mu Y, Wang X. 1,1′-Binaphthyl-2,2′-diamine as a novel MALDI matrix to enhance the in situ imaging of metabolic heterogeneity in lung cancer. *Talanta*. 2020;209:120557.
46. Stepka P, Vsiansky V, Raudenska M, et al. Metabolic and amino acid alterations of the tumor microenvironment. *Curr Med Chem*. 2021;28(7):1270–1289.
47. Vicente J, Fuster-Garcia E, Tortajada S, et al. Accurate classification of childhood brain tumours by in vivo ^{1}H MRS—a multi-centre study. *Eur J Cancer*. 2013;49(3):658–667.
48. Kohe S, Brundler M-A, Jenkinson H, et al. Metabolite profiling in retinoblastoma identifies novel clinicopathological subgroups. *Br J Cancer*. 2015;113(8):1216–1224.
49. Kato S, Bowman ED, Harrington AM, Blomeke B, Shields PG. Human lung carcinogen-DNA adduct levels mediated by genetic polymorphisms in vivo. *J Natl Cancer Instit*. 1995;87(12):902–907.
50. Osawa T, Shimamura T, Saito K, et al. Phosphoethanolamine accumulation protects cancer cells under glutamine starvation through downregulation of PCYT2. *Cell Rep*. 2019;29(1):89–103.
51. Lamore SD, Cabello CM, Wondrak GT. The topical antimicrobial zinc pyrithione is a heat shock response inducer that causes DNA damage and PARP-dependent energy crisis in human skin cells. *Cell Stress Chaperones*. 2010;15(3):309–322.
52. Li R-Z, Wang X-R, Wang J, et al. The key role of sphingolipid metabolism in cancer: new therapeutic targets, diag-

nostic and prognostic values, and anti-tumor immunotherapy resistance. *Front Oncol*. 2022;12:941643.

53. Dalle Vedove E, Costabile G, Merkel OM. Mannose and mannose-6-phosphate receptor-targeted drug delivery systems and their application in cancer therapy. *Adv Healthcare Mater*. 2018;7(14):e1701398.
54. Dachev M, Bryndová J, Jakubek M, Moučka Z, Urban M. The effects of conjugated linoleic acids on cancer. *Processes*. 2021;9(3):454.
55. Zhou D, Duan Z, Li Z, et al. The significance of glycolysis in tumor progression and its relationship with the tumor microenvironment. *Front Pharmacol*. 2022;13:1091779.
56. Takahashi H, Kawabata-Iwakawa R, Ida S, et al. Upregulated glycolysis correlates with tumor progression and immune evasion in head and neck squamous cell carcinoma. *Sci Rep*. 2021;11(1):17789.
57. Yerly L, Pich-Bavastro C, Di Domizio J, et al. Integrated multi-omics reveals cellular and molecular interactions governing the invasive niche of basal cell carcinoma. *Nat Commun*. 2022;13(1):4897.
58. Hwang S-H, Yang Y, Jung J-H, Kim Y. Oleic acid from cancer-associated fibroblast promotes cancer cell stemness by stearoyl-CoA desaturase under glucose-deficient condition. *Cancer Cell Int*. 2022;22(1):404.
59. Li L, Tian Y. The role of metabolic reprogramming of tumor-associated macrophages in shaping the immunosuppressive tumor microenvironment. *Biomed Pharmacother*. 2023;161:114504.
60. Bertero T, Oldham WM, Grasset EM, et al. Tumor-stroma mechanics coordinate amino acid availability to sustain tumor growth and malignancy. *Cell Metab*. 2019;29(1):124–140.
61. Cheteh EH, Augsten M, Rundqvist H, et al. Human cancer-associated fibroblasts enhance glutathione levels and antagonize drug-induced prostate cancer cell death. *Cell Death Dis*. 2017;8(6):e2848.
62. Akter Z, Salamat N, Ali MY, Zhang L. The promise of targeting heme and mitochondrial respiration in normalizing tumor microenvironment and potentiating immunotherapy. *Front Oncol*. 2022;12:1072739.
63. Prydz K, Dalen KT. Synthesis and sorting of proteoglycans. *J Cell Sci*. 2000;113(pt 2):193–205.
64. Mulder GJ. Glucuronidation and its role in regulation of biological activity of drugs. *Annu Rev Pharmacol Toxicol*. 1992;32:25–49.
65. Doshi MB, Lee N, Tseyang T, et al. Disruption of sugar nucleotide clearance is a therapeutic vulnerability of cancer cells. *Nature*. 2023;623(7987):625–632.
66. Brewer G. UXS1: a sweet spot for cell death. *Nat Rev Cancer*. 2024;24(1):3.
67. Wu X, Elkin EE, Marghoob AA. Burden of basal cell carcinoma in USA. *Future Oncol*. 2015;11(22):2967–2974.
68. Zhao J, Jin D, Huang M, et al. Glycolysis in the tumor microenvironment: a driver of cancer progression and a promising therapeutic target. *Front Cell Dev Biol*. 2024;12:1416472.
69. Goldenberg G, Karagiannis T, Palmer JB, et al. Incidence and prevalence of basal cell carcinoma (BCC) and locally advanced BCC (LABCC) in a large commercially insured population in the United States: a retrospective cohort study. *J Am Acad Dermatol*. 2016;75(5):957–966.
70. Bisceglia M, Panniello G, Galliani CA, et al. Metastatic basal cell carcinoma of the skin: a comprehensive literature review, including advances in molecular therapeutics. *Adv Anatomic Pathol*. 2020;27(5):331–353.